ORIENTAL JOURNAL OF CHEMISTRY
An International Open Access, Peer Reviewed Research Journal
www.orientjchem.org
ISSN: 0970-020 X
CODEN: OJCHEG
2025, Vol. 41, No.(2):
Pg. 675-688

Potential Utilization of Eco Benign Material as Effective Divalent Ions Encapsulant from Aqueous Matrix and Industrial Effluent

DHARANI SELVAKUMAR[1] and MUTHULAKSHMI ANDAL NARASIMHAN[2]*

[1,2]Department of Chemistry, PSGR Krishnammal College for Women, Coimbatore-4, India.
*Corresponding author E-mail: muthulakshmiandal@psgrkcw.ac.in

http://dx.doi.org/10.13005/ojc/410237

(Received: February 22, 2025; Accepted: April 09, 2025)

ABSTRACT

Release of toxicants from multiple sectors into water streams cause adverse effects in the environment. In recent years, due to their great persistence and toxic nature, heavy metals are considered as a major threat generated from diverse industrial units. Amongst various pollutants, high level of heavy metal (Zn, Pb, Hg, Ni, Cu & Fe) contamination create numerous health hazards like immune system dysfunction, gastrointestinal problems, birth defects, nervous disorders and thereby affecting surface water quality. This study is centred on the preparation of magnetite composite using chemically Treated Anas platyrhyncos Legs Powder (TALPMC) as a precursor to abstract Zn(II) and Pb(II) ions aqueous media. Metal sequestering ability of the treated powder (TALP) and prepared magnetite composite (TALPMC) were studied via pilot method. Batch Equilibration verification was done for TALPMC to optimize the influential parameters viz., particle sizes, sorbent dose, initial concentration of sorbate species, time interval, pH and temperature, so as to regulate the sorptive effectiveness. Microscopic analysis, BET/BJH, FT-IR, SEM/EDAX, TG-DTA and XRD studies were conducted to characterize the physical and chemical nature of the material. Initial and residual experimental run concentrations of metal solutions were interpreted using Atomic Absorption Spectrophotometer. Sorption capacity of TALP (89% Zn(II) and 85% Pb(II)) was observed to multiply by homogenizing it with the prepared magnetite, this resulted in 97% Zn(II) and 95% Pb(II) removal. Desorption and regeneration experiments were performed to examine the reusable nature of exhausted TALPMC. Electrostatic attraction between Zn^{2+} and negatively charged surface of TALPMC shall be the ascertained reason. Upon derived plots isothermal studies, most linear fit of Langmuir isotherm favoured monolayer sorption. Kinetic studies revealed the applicability of pseudo-second order model. As per the results obtained from Batch Optimization assay, extensive quantity of toxicants was immobilized by TALPMC than TALP. Thus, to ascertain the efficacy of TALPMC against industrial discharges, effluent sample was collected from oil industry and a pilot study was performed for magnetite systems. Trapping of 92% Zn(II) and 88% Pb(II) ions from the raw sample was registered by TALPMC. From the made observations, it is concluded that TALPMC serves as an excellent metal scavenger against its precursor.

Keywords: Magnetite, Precursor, Batch, Zinc, Lead, Sorption.

INTRODUCTION

Industries use water resource for countless operations such as coolant in power plants, solvent in oil refineries and in other manufacturing units[1]. Exponential rise in water scarcity is due to expansion of urbanization and industrial operations[2]. 22% of available water sources is consumed by industries and released directly into water bodies[3]. Oils, greases, dyes, acids, alkalis and noxious heavy metals are few prominent materials present as toxicants in water[4]. These are non-biodegradable and progressively accumulate in the food chain[5], thereby increasing their concentrations in living organisms over time[6]. Therefore, water quality maintenance is extremely required to meet the global usability and scarcity of water resources[7]. Of these, oil producing plants vent out chemicals, which deplete oxygen, stimulate the growth of pathogens and affect the marine ecosystem[8]. Many methodologies have been endorsed in the process of scavenging these metal ions, of which adsorption is found to be the most operative method because of its selectivity, feasibility and effectiveness, whereas other reformative techniques generate large amounts of sludge which destroy surrounding environs and their handling is very expensive. Pollutants discharged by the oil yielding companies generally contain heavy metals like Cd, Pb, Cu, Fe and Zn. Of these distinct toxicants, abstraction of Zinc and lead ions under laboratory set up employing treated and magnetic sorbent is eventually explained in this work, because of the permissible limit that exceeds slightly in the effluent collected from the concerned industry. Prevalence of heavy metals in oil may be due to contamination that occurs during the collection of seeds, addition of excess fertilizers to soil, plants that affects its metabolic processes or by the procedures employed during oil extraction.

Zinc, the essential element for many physiological reactions that eventuate in human body, thus promoting metabolism and functioning of immune system[9]. But when surplus amount of zinc (used in food preservation, agriculture, food processing industries etc), consumed via food, cause serious health hazards. Inspite of its widespread applications, excess of zinc ions perturbs human health, causing gastrointestinal disorders, infections in respiratory tract, epigastric pain and other neurological defects[10].

Lead is the highly poisonous metal, affecting almost every organ in the body. Existence of lead ions in pipes, that are employed in the industrial process has a direct or indirect influence in polluting ground water resources[11]. Thus, long-time exposure to lead can cause anaemia, thereby increasing blood pressure. Severe damage to the brain and kidneys, results in death[12]. In pregnant women, high exposure to lead may cause miscarriage. Chronic lead exposure results in the reduction of fertility in males[13].

Naturally available minerals, biopolymers and nanoparticles have been reported in literature to treat these oil effluent discharges[14]. The present investigation is focussed on synthesizing magnetite composite using (AL) as precursor, followed by evaluating its adsorbing ability upon zinc and lead ions in aqueous environs. The choice of eco litter material is based on its widespread availability, financial feasibility apart from non-being reported elsewhere in exploring its adsorption properties. Sorption capacity of Anas platyrhyncos Legs was found to be efficient in chelating heavy metals in comparison with other animal bone wastes[15], investigated by N. A. Medellin-Castillo *et al.,*

MATERIALS AND METHODS

Collection and Modification of Sorbent

Anas platyrhyncos is a variety of duck species, classified under family Anatidae. It is a popular form of poultry and raised throughout temperate parts of Tamil nadu as a part of industrialized farming, making it viable for the edible meat consumption. However, the legs of these ducks are thrown as litter. They were gathered from various localities of Nammakal district, familiar for poultry activities. The collected legs were washed thoroughly and the leg bones were carbonized in an oven (300°C for 2 h) and later dried (Fig. 1). The parched material was crushed, powdered in an electrical mixer (Fig. 2) and categorized into different mesh sizes (85BSS, 72BSS, 52BSS, 36BSS and 22BSS). Further, appropriate doses of these materials were transferred to a beaker containing 100mL of 0.1 N HCl and heated for 3 hours. The same procedure was repeated using 0.1 N NaOH. This chemical

modification ensured the enhancement of their surface properties, thereby reflecting upon metal sorbing capacities.

Synthesis of Magnetite

Ferrous and ferric chloride salts were mixed in 1:2 ratio and dissolved in 5 mL distilled water. The yellowish brown mixture was agitated well using magnetic stirrer until it turned to reddish brown hue. Few drops of NaOH solution was added to produce iron oxides and to ensure complete dissolution. The forms black magnetite precipitate was left behind (Fig. 3) undisturbed for few hours to assure absolute formation of Fe_3O_4. Colour of the magnetite depends on the intervalence charge transfer between Fe^{2+} and Fe^{3+} in its crystal structure[16].

Preparation of Anas platyrhyncos Legs Powder Magnetite Composite (TALPMC)

7 gram of TALP precursor was suspended in a volume of 20 mL prepared magnetite solution. This was stirred for 45 min to obtain a homogeneous mix of Anas platyrhyncos legs powder magnetite composite, labelled as TALPMC (Fig. 4). The derived magnetic composite was decanted, dehydrated (80°C) and stored for further analyses.

Fig. 1. Anas platyrhyncos Legs (AL)

Fig. 2. Treated AL Powder (TALP)

Fig. 3. Magnetite

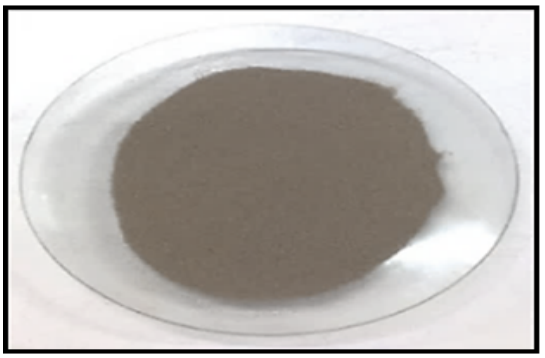

Fig. 4. TALP Magnetite Composite (TALPMC)

Adsorbate Solutions Preparation

Specific amounts of zinc sulphate and lead nitrate salts (Sigma Aldrich) were dissolved in 1000 mL double distilled water and labelled as stock solutions. Appropriate dilutions of these stock solutions were done to prepare 100 mg/L standards. Further, aliquots ranging from 5-25 mg/L: 5 mg/L were made up in respective standard flasks.

Pilot Study

Batch Equilibration studies were designed to assess the metal trapping capacity of the sized materials. 50 mL of 50 mg/L Zn(II) and Pb(II) solutions were agitated for 30 min with 1 g dose of treated (TALP) and its magnetic counterpart (TALPMC). Better metal confiscation is observed for TALPMC rather than its treated precursor as given in Table 1. The Batch reaction conditions were optimized for both the materials, since they unveiled notable percentage removal in the pilot studies.

Table 1: Removal of Divalent ions-Pilot study

Materials	% Removal Zn(II)	Pb(II)
TALP	73.2	71.3
TALPMC	78.4	76.2

Characterization Studies

Native, treated and magnetite sorbents were subjected to characterization studies using Ultrasound microscope, BET/BJH, FTIR, SEM/EDAX, TG-DTA and XRD, so as to determine their structure, surface area/porous nature, involvement of functional groups, composition of elements both in unloaded and metal loaded materials, thermal behaviour and crystallinity of the magnetic sorbent. Binocular Ultrasound microscope (OLYMPUS make, Model-CX21I) was used to determine the particle sizes. Bruner-Emmet-Teller (BET) and Barrett-Joyner-Halenda (BJH) plots were used to determine the surface areas and porous nature of the modified precursors, equipped with Adsorption /Desorption data analysis software. Participation of functional groups in the sorption process was studied using Fourier Transform Infrared Spectrophotometer (Shimadzu). Scanning Electron Microscope (SEM) and Energy Dispersive X-ray Spectrometer (EDAX) spectra of ZEISS make were recorded to signify surface morphological changes and framework of the metal laden and unloaded counterparts. TG/DTA curves were derived using NETZSCH JUPITOR STA 449F3 for analysing the thermal stability, mass loss and composition of the material at varying temperatures. Crystalline nature of the magnetite sorbent was estimated by XRD of Bruker D8 Advance make, λ = 0.154 nm.

Batch Equilibration Studies

Sorption efficiencies of the four systems viz., Zn(II)-TALP; Zn(II)-TALPMC; Pb(II)-TALP and Pb(II)-TALPMC were optimized with underlying factors viz., particle size (0.18, 0.21, 0.30, 0.42, 0.71 mm); initial sorbate concentrations (5-25 mg/L : 5 mg/L); Dose (10-60 mg : 10 mg); agitation time period (3-30 mins: 3 mins). Batch experiments were designed in such a way that the specified dose of both the materials being added to a 250 mL Erlenmeyer flasks containing standard volume of 50 mL Zn and Pb solutions of specified concentrations. Under the predetermined circumstances, the contents of the flask were shaken in a mechanical shaker (KEMI model) at a speed of 140 rpm. Later, these samples were filtered, analysed for initial and residual metal concentrations using Atomic Absorption Spectrophotometer (Shimadzu (AA 6200) model) at the corresponding wavelengths of 213.9 nm and 324.8nm for Zn(II) and Pb(II). Role of key parameters like pH (ELICO (LI-120) pH metre) 3,5,7,9,11 and temperature (TECHNO thermostat-controlled incubator shaker) 293-333 K:10K were listed for Zn(II)-TALPMC and Pb(II)-TALPMC systems under fixed conditions, since these factors play a vital role in controlling the concentration and mobility of sorbate ions in the solution.

Desorption/Regeneration Experiments

Adsorption/desorption studies were conducted to evaluate the sustainable nature of TALPMC against aqueous/industrial effluents, thereby promoting economic viability of the process. An effectual desorption procedure includes appropriate eluent selection to desorb the sorbent species and sorption mechanism. The strength of desorbing medium (HCl) was fixed as 0.01N because of its ability to subside the desorption rate, indicating maximal sorbent redemption at various consecutive cycles.

Pilot Study–Oil Effluent Sample

The results obtained from pilot study being in favour of the sequestering ability of TALPMC has led to focus on the up scaling of the material's applicability to abstract the specified divalent ions from raw effluent sample. However, the choice of heavy metals (Zn & Pb) for the present study was deliberately based on their inclusive occurrence in the oil effluent, transcending the permissible limits. In this context, effluent sample was collected from oil refinery located at Karur, Tamil Nadu, India. Metal concentrations in the collected oil effluent sample analysed using Atomic Absorption Spectrophotometer (AAS) within the corresponding wavelengths and slit width exposed their intensities as to exceed the prescribed tolerance levels (WHO Standards). In order to align with the tested aqueous metal solution concentrations, the sample was processed as follows:

500mL of the sample was poured into a beaker, heated to 80°C for 30 min, followed by the addition of 5N conc. H_2SO_4, to separate the sludge from the boiled sample. Later, extraction procedure was done to discard the sludge, and the sample was diluted to explicit concentrations. 50 mL of the thinned samples were transferred into 250 mL flasks, followed by the addition of TALPMC dose (10-50mg: 10 mg) agitated (120 rpm) in a shaker at preset time intervals (5-30: 5 mins) and filtered. Metal residual concentrations of the sorted and that of the pre-run samples were determined.

Adsorption Isotherms and Kinetics

Adsorption data were graphically determined for Zn(II)-TALPMC & Pb(II)-TALPMC systems, based on the optimized results. Langmuir, Freundlich and Tempkin isotherms models were taken into account to validate and predict the interaction between sorbate ions (Zn(II) & Pb(II)) and sorbent surface (TALPMC). Also, the sorbing efficiency of chosen sorbent against cations was determined using pseudo-first-order and pseudo-second-order kinetic models.

RESULTS AND DISCUSSION

Microscopic Studies

Range of porosity in descending order, is represented in Fig. 5(a) to 5(b). Modified TALP and prepared TALP magnetite composite (Fig. 5(c)) appear to possess granular pore size, with varying fineness than their natant material. This would be due to opening of cavities during acid/base treatment and enabling the formation of magnetite complex respectively.

Fig. 5a. ALP

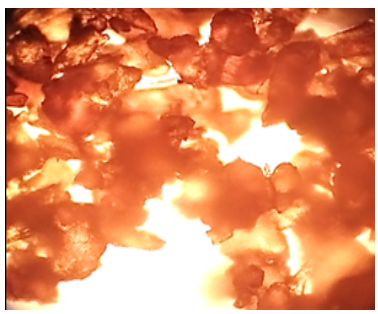

Fig. 5b. TALP

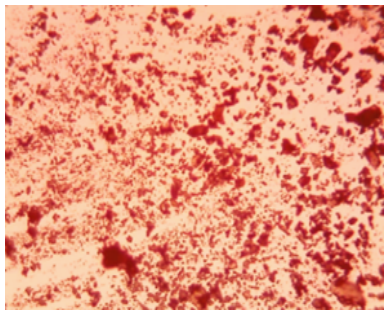

Fig. 5c. TALPMC

BET/BJH

BET/BJH graphs (Fig. 6 & 7) clearly show the total specific exterior TALPMC surface area, internal pore volume and pore size distribution data as depicted in Table 2. Adsorbents for liquid phase adsorbate should be mesoporous to accommodate bigger liquid molecules. The type IV adsorption-desorption isotherm (Fig. 8), which shows its textural feature, demonstrates the mesoporous nature with significant surface area. A narrow porous matrix with a wide capillary width and a non-uniform size is preferred by the pore size distribution pattern, which is centred at 5 nm. Aggregates of plate-like particles with slit pores are represented by a meagre broad H3 type hysteresis loop (clear hysteresis at P/P°> 0.6).

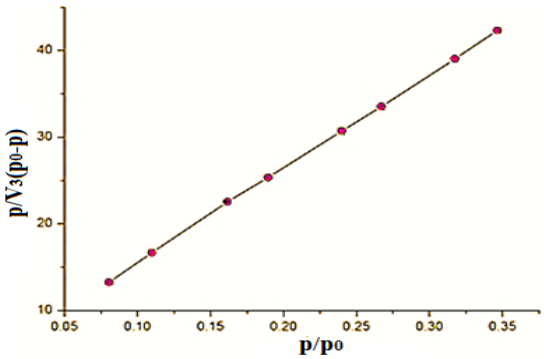

Fig. 6. BET plot

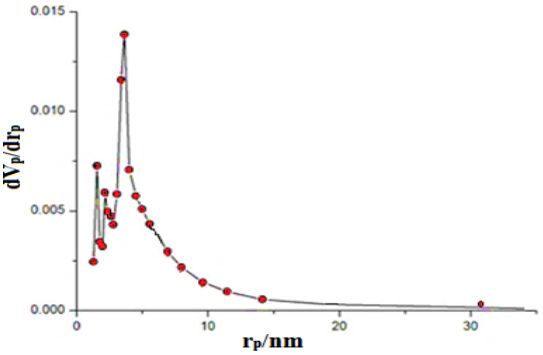

Fig. 7. BJH plot

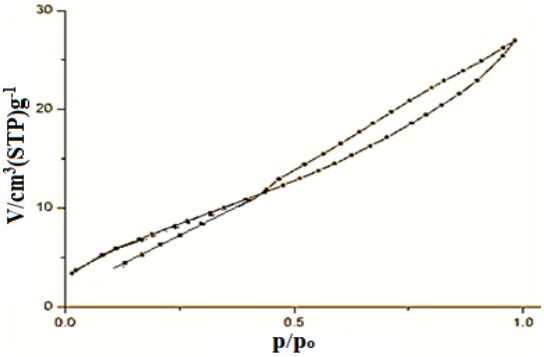

Fig. 8. Adsorption/Desorption Isothermal Plot

Table 2: BET/BJH parameters

Specific surface area (m^2/g)	30.85
Pore size distribution (nm)	5
Total pore volume (cm^3/g)	0.45

FT-IR

Pre and post run spectra of TALP are shown in Fig. 9(a). Notable bands around 700 cm^{-1} and sharp peak at 1410 cm^{-1} in sorbate ions loaded TALP indicate the participation of Ca ions in sequestering the divalent cations. Broad band shift from 3525 cm^{-1} in TALP to 3484 cm^{-1}, 3437 cm^{-1} in loaded spectra confirm the stretching of alcoholic –OH group. A sharp peak at 1020 cm^{-1} and 1017 cm^{-1} imply the C-O stretching to adsorb Zn(II) and Pb(II) ions. Involvement of alkane group (C-H stretching) in modified and metal sorbed materials is evident from corresponding peak shift from 2696 cm^{-1} to 2908 and 2904 cm^{-1}.

FTIR spectra of magnetite complex and its laden counterparts are depicted in Fig. 9(b). Band at 3514.8 cm^{-1} for OH group, indicate the presence of alcoholic –OH group in the precursor. Appearance of new peaks at 2927 cm^{-1} & 2922 cm^{-1} in the metal laden counterparts denote that the stretching of C-H bonds in alkane group had occurred in the native material. Bands at 1400 cm^{-1} and 1080 cm^{-1} refer to the contribution of Ca^{2+} ions towards sorption of divalent ions, where replacement of cations (Zn^{2+} and Pb^{2+}) by calcium ions occur on the sorbents' surface (ion exchange mechanism), thereby extracting the divalent ions from the solution. New peaks at 1706 cm^{-1} and 1704 cm^{-1} in the metal loaded sorbents reveals C=C bending in TALPMC. A prominent band around 580 cm^{-1} confirms the binding of Fe_3O_4 to the treated material. The chelating efficiency of TALPMC against Zn(II) and Pb(II) is further proved by broad and intense bands at 580 cm^{-1} in metal laden spectra. Thus, variation and shift in the peaks shows the involvement of functional groups during the sorption process.

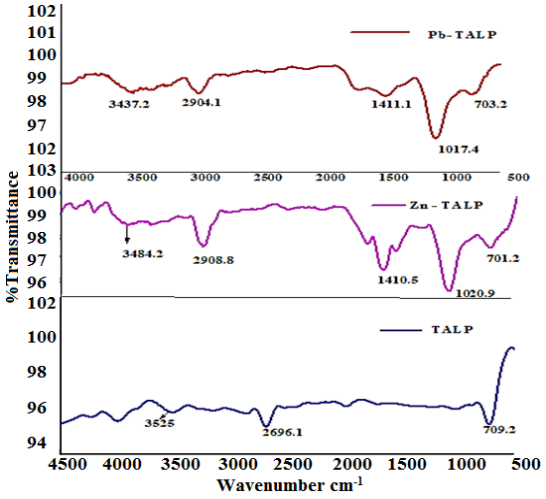

Fig. 9(a). TALP, Zn(II)-TALP, Pb(II)-TALP

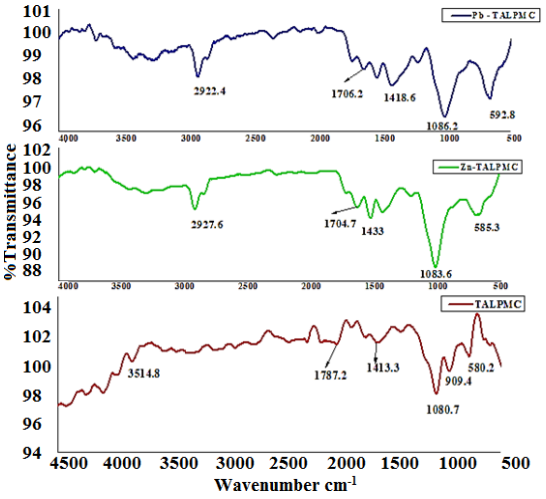

Fig. 9(b). TALPMC, Zn(II)-TALPMC, Pb(II)-TALPMC

Surface Topographical Investigation (SEM/EDAX)

Rough surface pores of activated sorbent, TALP (Fig. 10(a)) is uniformly occupied by Zn(II) (Fig. 10(b)) and Pb(II) ions (Fig. 10(c)) clusters. Rod shape arrangement in TALPMC (Fig. 11(a)) substantiates marked changes from its appearance in Fig. 10(a), which may be due to the augmentation of magnetite within the treated matrix (TALP). Post run images of the magnetite fused sorbent (Fig. 11(b) & 11(c)) depicts the filling up of the open apertures by the respective sorbate ions, confirming their uptake.

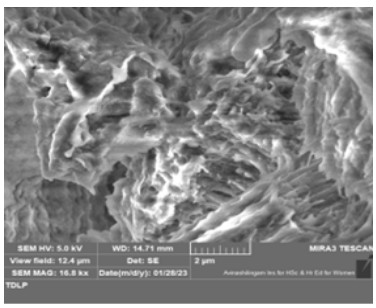

Fig. 10(a). TALP

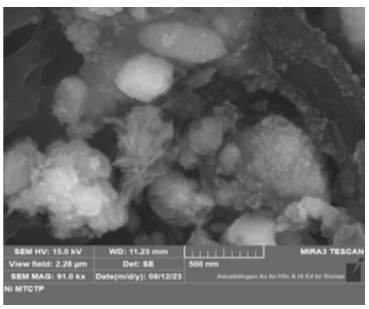

Fig. 10(b). Zn(II)-TALP

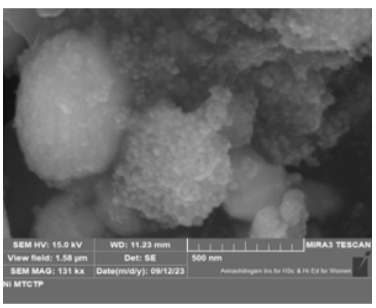

Fig. 10(c). Pb(II)-TALP

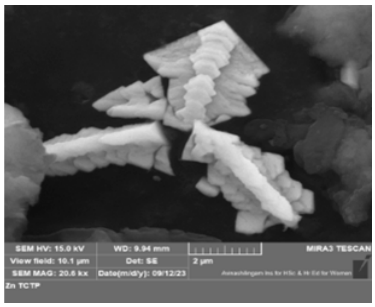

Fig. 11(a). TALPMC

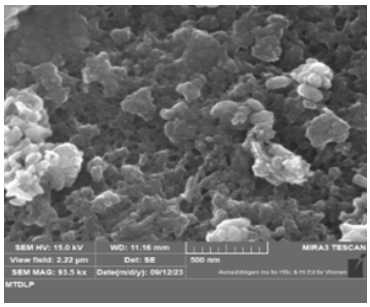

Fig. 11(b). Zn(II)-TALPMC

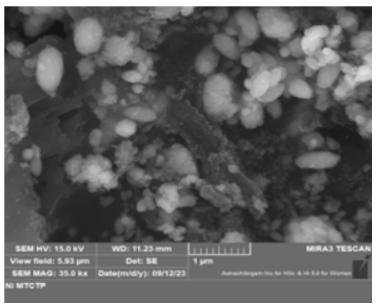

Fig. 11(c). Pb(II)-TALPMC

EDAX image (Fig. 12a) depicts a peak at 7KeV corresponding to Cl atom, the presence of which shall be due to acid/base treatment of the raw material. Popping up of new peaks between 4-6 KeV is obvious from Fig. 12b & 12c, favouring the respective sorption of divalent ions. Prominent peaks in all EDAX images representing Ca ion further support the results envisaged in FT-IR spectra. Peaks at 6-8 KeV in Fig. 13a refers to Fe^{2+} ion, thereby ensuring its coherence within TALP to form the magnetite. Additional peaks at 5KeV and 2KeV in Fig. 13b & 13c confirm the adhesion of divalent ions onto the sorbent layer.

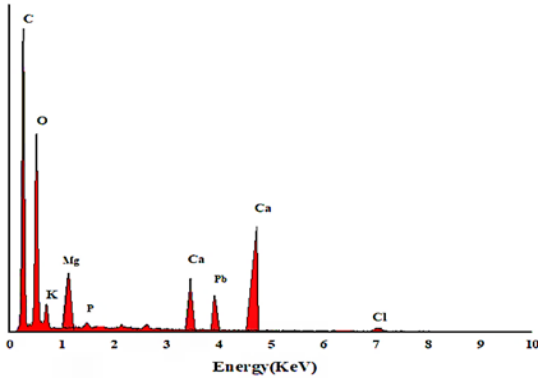

Fig. 12c. Pb(II)-TALP

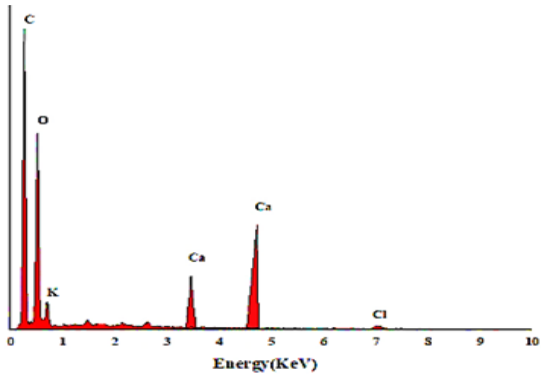

Fig. 12(a). TALP

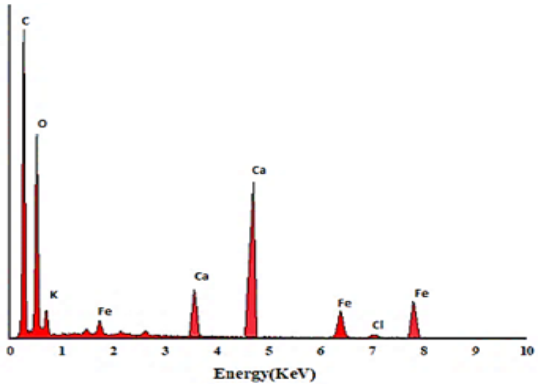

Fig. 13(a). TALPMC

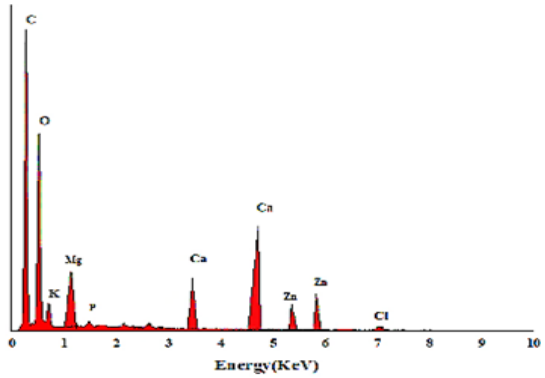

Fig. 12(b). Zn(II)-TALP

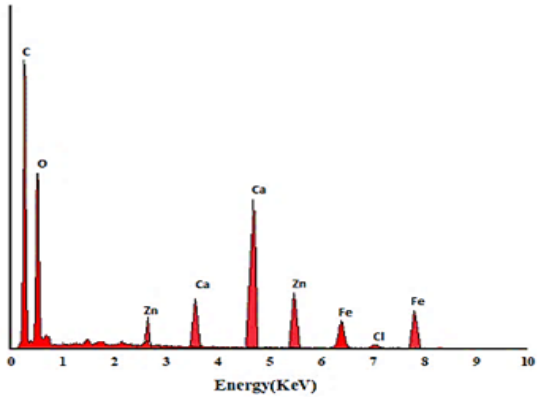

Fig. 13(b). Zn(II)-TALPMC

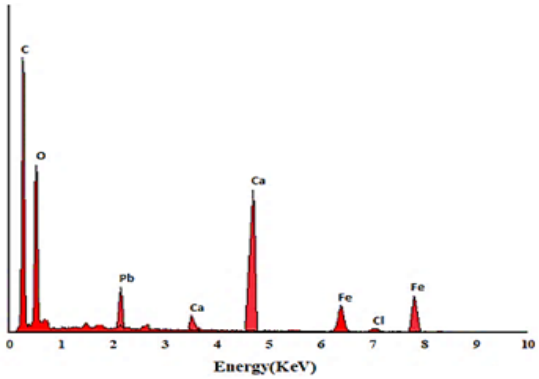

Fig. 13(c). Pb(II)-TALPMC

TALPMC was subjected to TG-DTA and XRD studies to determine its thermal stability, magnetic nature and crystallinity.

Thermal Analysis–TG /DTA

Thermogram (Fig. 14) represents the thermal degradation behaviour at two regions of varied temperature conditions ranging from 100-600°C. Endothermic curve (red curve) at 100°C depicts moisture evaporation. The broader exothermic curve (300-400°C) imputes the decomposition of organic materials viz., collagen and minerals found in Anas platyrhyncos bones. A steady declined curve observed beyond 400°C, indicates the carbonization of magnetite under controlled air atmosphere.

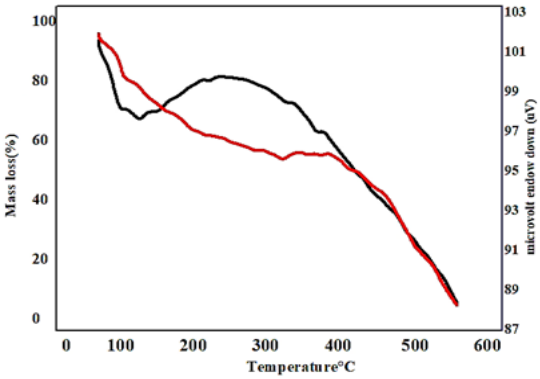

Fig. 14. TG/DTA–TALPMC

X-ray Diffraction Analysis

Figure 15 represents the XRD pattern with broad peaks of less sharpness, predicting TALPMC's amorphous nature at room temperature. This powdered characteristic shall be recognized as the presence of organic matter in the magnetite. Characteristic peaks of Fe_3O_4 at 2θ as 30.1, 35.6, 43.2, 53.4, 57 and 62.7 relate to the planes (220), (311), (400), (422), (511) & (440), as per JCPDS card number: 85-1436. Infusion of Anas platyrhyncos Leg bones as precursor in the magnetite composite is further confirmed by the appearance of peaks at 2θ angle (25.11, 38.8 and 49.5), referring to Hydroxy APatite (HAP), thereby proving the existence of Ca ions.

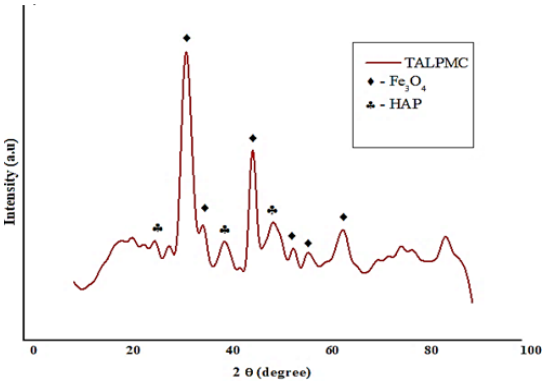

Fig. 15. XRD-TALPMC

Batch Optimization Studies

Influence of Particle Size

Particle size has a major impact on its sorption effectiveness towards any noxious substance. Fig. 16a and 16b portray the chelating efficacies of derived materials at varying sizes. 0.18 mm of treated and magnetite based sorbent possess greater potential to confiscate divalent ions, evident from the varied bar height as 89% zinc, 85% lead ions (Fig. 16a) and 97% Zn(II), 95% Pb(II) ions (Fig. 16b). This shows that the sorbent with reduced size has expanded surface area, thence 0.18mm particle size was fixed for further experimental studies.

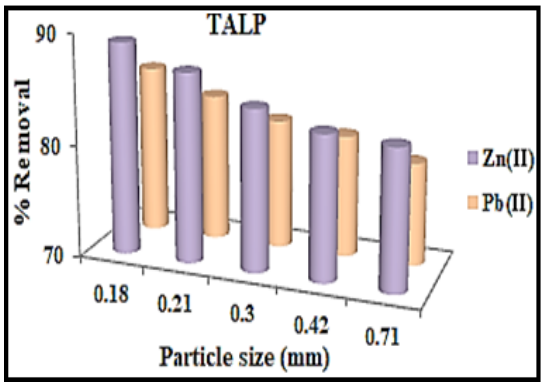

Fig. 16(a). Particle Size – TALP

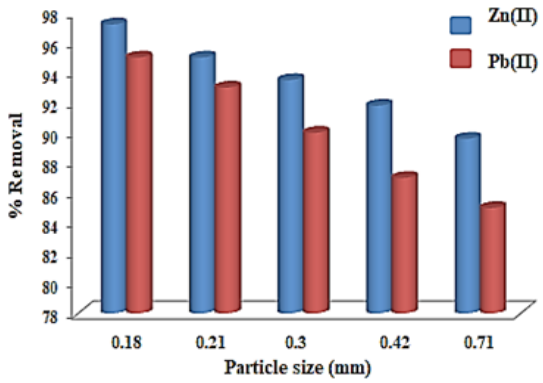

Fig. 16(b). Particle Size-TALPMC

Influence of Initial Concentration on Time

Sorption ability of TALP is demonstrated in Fig. 17a & 17b. Acquisition of active sites on TALP by Zn(II) and Pb(II) ions had occurred at 21 mins for 10 mg/L corresponding solutions. Rapid adsorption of Zn (89%) and Pb (85%) appeared initially and as the contact time boosts up, the ability of TALP grasping the sorbate species diminished, leading to agglomeration, sufficed by the trend of the curves.

Figures 18a & 18b pictures the effect of sorbate concentrations at periodic time intervals on TALPMC. Orderly distribution of Zn(II) and Pb(II) ions on the surface of the magnetite sorbent had occurred at 15 mins for concentrations of 10 mg/L and 15 mg/L. Utmost removal of zinc and lead ions had appeared at 97% and 95.1%, exhibited from the inverted parabolic curves. A decline in the sorption pattern is noticed while increasing the metal concentrations, accounting for a biased desorption of divalent ions on the solid matrix due to saturation of active sites.

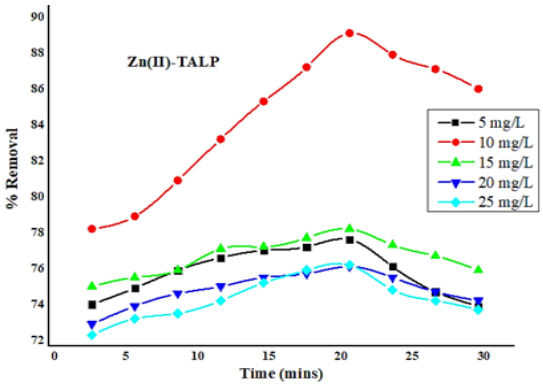

Fig. 17(a). Initial Concentration on Time–Zn(II)-TALP

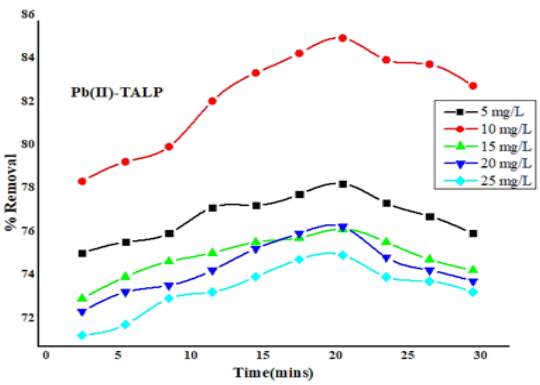

Fig. 17b. Initial Concentration on Time–Pb(II)-TALP

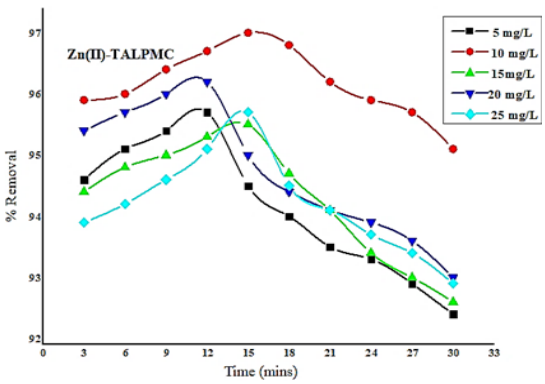

Fig. 18(a). Initial Concentration on Time–Zn(II)-TALPMC

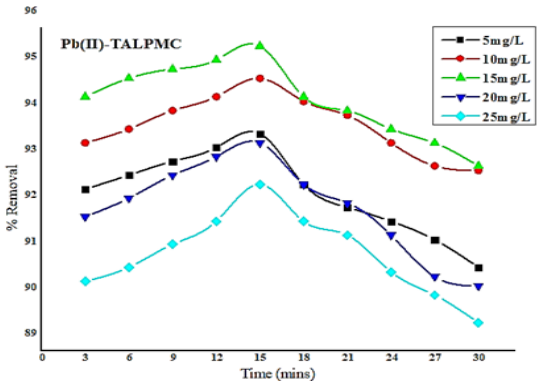

Fig. 18(b). Initial Concentration on Time–Pb(II)-TALPMC

Influence of TALP and TALPMC Dosage

Variations of doses (10 mg to 60 mg: 10 mg) are depicted in Fig. 19a, 19b & 20a, 20b. Bare orifices on surface pores of TALP had been captured by the divalent ions. The conditions optimized for maximal metal sequestration (Zn(II)-89.4% & Pb(II)-85.3%) are 50 mg TALP and 18 mins agitation time frames as manifested from Fig. 19a & 19b. However, a better inclined pattern is visible from the parabolic curves (Fig. 20a & 20b) reveals that the optimal TALPMC doses required were 30 mg & 40 mg for dispensing the capture of 97% Zn(II)

and 95% Pb(II) ions respectively. Both the reactions registered uttermost metal abstraction within a time frame of 15 minutes. Decline in the curves, beyond the optimum dosage, imply aggregation of sorbent moieties at higher doses resulting in the decreased metal uptake.

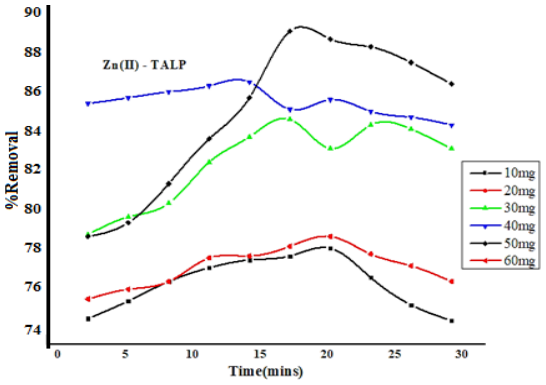

Fig. 19(a). Influence of Dose Zn(II)–TALP

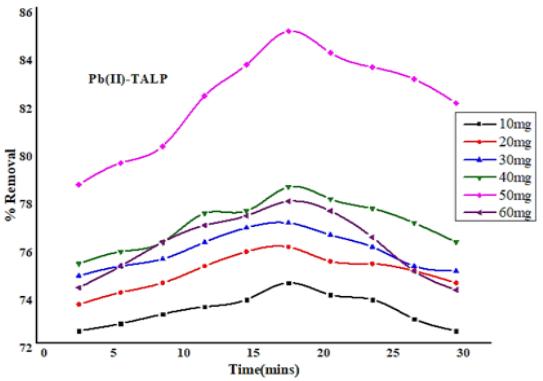

Fig. 19(b). Influence of Dose Pb(II)–TALP

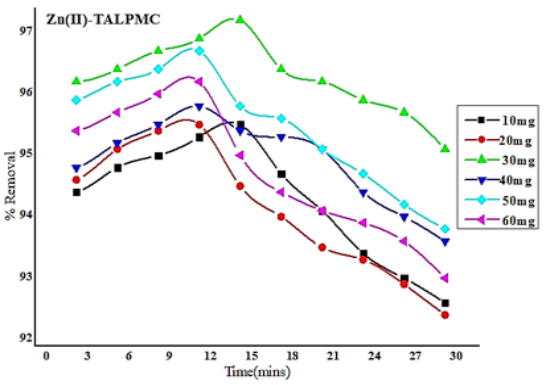

Fig. 20(a). Influence of Dose Zn(II)-TALPMC

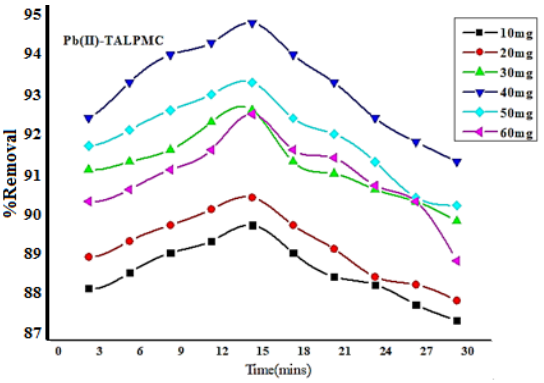

Fig. 20(b). Influence of Dose Pb(II)–TALPMC

From the made observations, it is evident that the chelation of divalent ions by TALPMC proved to be better than its precursor TALP. Hence, fixing of other parameters such as pH and temperature was limited to TALPMC systems.

Influence of pH

pH impact on any adsorption system plays a pivotal role, since the abstraction activity of the material can be enhanced in acidic/basic environments. In this context, removal of Zn & Pb ions under varied pH environs was studied and the resulting data is illustrated in Fig. 21. It is obvious from the figure that, Zn(II) removal had reached its pinnacle at pH 5, due to less competency between acidic H^+ and metal cations at higher pH. This facilitates greater occupation of Zn(II) ions on the vacant sites of TALPMC. Thus, effective sorption is adhered, reflecting the deprotonation of carboxylic groups[15]. Utmost Pb(II) acquisition had occurred at pH 7. At higher alkaline pH, the divalent ions get precipitated as hydroxides, diminishing TALPMCs' quenching ability. Also, increasing amount of Na^+, in basic medium competes with Zn^{2+} & Pb^{2+} ions to get preferentially sorbed on exchangeable active sites available on TALPMC surface.

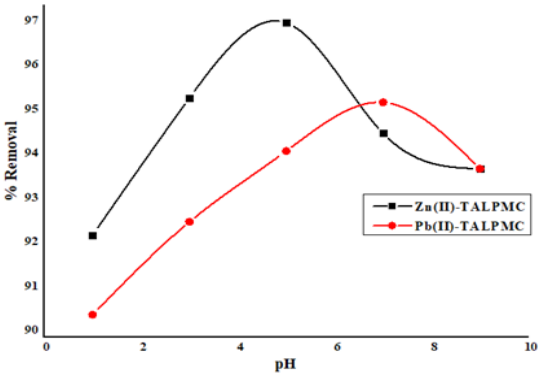

Fig. 21. Influence of pH

Influence of Temperature

Temperature studies expose its inverse

relation against metal removal (%) as evident from Fig. 22. Notable confiscation of Zn^{2+} (97.3%) & Pb^{2+} (95.1%) ions had occurred at 303K, and 313K respectively. Limited availability of active centres at lower temperature and desorbing nature of metal ions from the magnetite surface at elevated temperatures has reflected in the percentage drop, under respective thermal conditions.

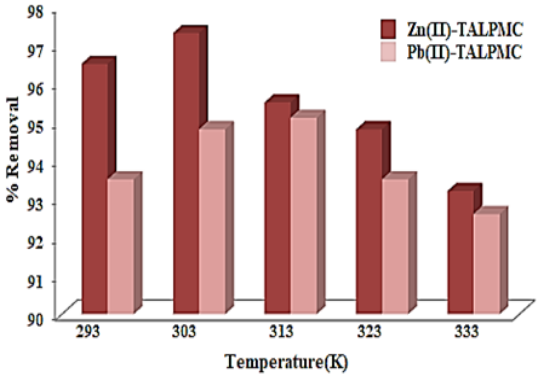

Fig. 22. Influence of Temperature

Desorption/Regeneration

Desorption capability and regenerating capacity of metals (Zn^{2+} & Pb^{2+}) loaded TALPMC were analyzed for three continuous cycles, followed by Batch Optimization studies. Marked variations in adsorption/desorption cycles of spent sorbent are depicted in Table 3 and it was found to be more pronounced for Zn(II)-TALPMC than Pb(II)-TALPMC system.

Sorption Isotherms

Batch experimental data were validated using Langmuir, Freundlich and Tempkin isotherms, wherein their constants/correlation coefficients (R^2) were computed from the corresponding plots. Table 4 shows that Langmuir constant q_m is considerably higher than the K_F, Freundlich constant, as far as both the systems are concerned. Free energy constant [b (L/g)] for the magnetite systems were found to be petite (0.26 and 0.17), inferring appreciable affinity of TALPMC to adsorb divalent ions. This favours the better linear fit of Langmuir model (Fig. 23), suggesting monolayer adsorption and homogeneous distribution of active sites on TALPMCs' surface. Further, it is evident from Freundlich model (Fig. 24), that the process is physical in nature, since 1/n values are greater than 1. Fig. 25 represents Tempkin isotherm, with greater B_T and lower A_T derived values. This reflects feeble applicability of this model to explain the interaction between sorbate ions and sorbent. In addition, calculated parametric values from graphical plots of all the three isotherms, reveal that TALPMC exhibited better encapsulation of Zn(II) than Pb(II).

Table 3: Desorption/Regeneration Studies

Systems	Cycle 1 (mg/g) Adsorption	Cycle 1 (mg/g) Desorption	Cycle 2 (mg/g) Adsorption	Cycle 2 (mg/g) Desorption	Cycle 3 (mg/g) Adsorption	Cycle 3 (mg/g) Desorption
Aq. Zn(II)-TALPMC	65.321.56	63.25	1.20	60.58	0.98	
Aq. Pb(II)-TALPMC	60.15	2.76	58.68	3.59	54.28	3.72

Table 4: Isothermal Constants

Isotherms	Parameters	Zn(II)-TALPMC	Pb(II)-TALPMC
	q_m (mg/g)	32.15	29.36
Langmuir	b (L/g)	0.2635	0.1789
	R^2	0.9960	0.9526
	K_F (mg/g)	5.45	3.26
Freundlich	1/n	1.64	1.42
	R^2	0.8677	0.8329
	A_T (L/g)	0.15	0.11
Tempkin	b_T	370.50	265.301
	R^2	0.7389	0.642 5

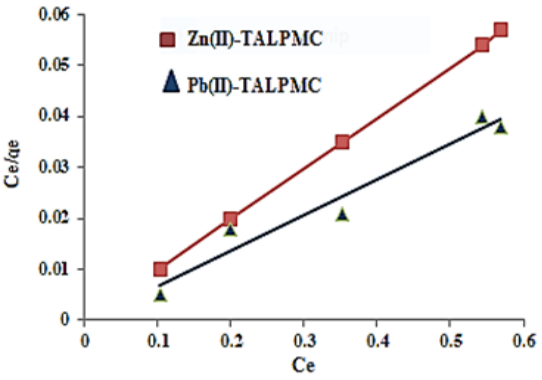

Fig. 23. Langmuir Model

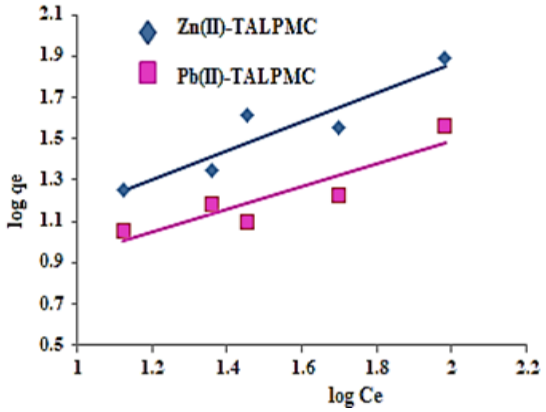

Fig. 24. Freundlich Model

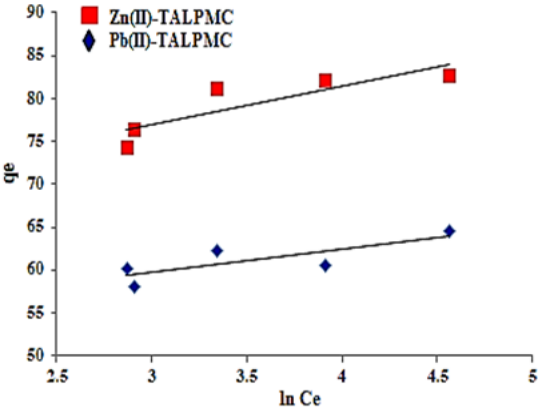

Fig. 25. Tempkin Model

Pseudo Kinetics

Data for pseudo-first and second order kinetic models at optimum concentrations within time frames (3 to 30 mins: 3 mins) enlisted in Table 5 were derived from the slopes and intercepts of the plots. Corresponding graphs (Fig. 26 & 27) were drawn using the kinetic equations [log ($q–q_t$) vs t, t/q_t vs t]. The q_{cal} value is greater for 10 mg/L Zn(II) & 15 mg/L Pb(II) concentrations, ensuring the effective metal ablating nature of magnetite composite. The better fit of second order model than its first order counterpart, is sufficed by the K_2 value, marginally lower than K_1 and R^2 value close to unity. Further, the aforesaid statement was supported by lesser SSE values obtained from respective linear plots.

Table 5: Kinetic Parameters

Systems	Pseudo first order				Pseudo second order			
	q_{cal} (mg/g)	$K_1 \times 10^{-3}$ (min^{-1})	R^2	SSE	q_{cal} (mg/g)	$K_2 \times 10^{-3}$ (min^{-1})	R_2	SSE
Zn(II)-TALPMC	34.52	13.74	0.8730	5.42	38.53	6.32	0. 9708	1.06
Pb(II)-TALPMC	32.42	10.31	0.7706	7.16	35.65	5.16	0.8585	2.25

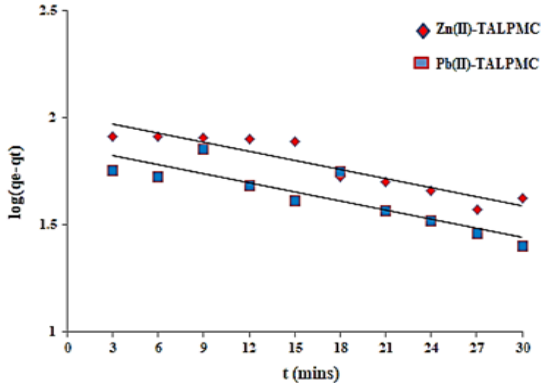

Fig. 26. Pseudo-First Order Kinetics

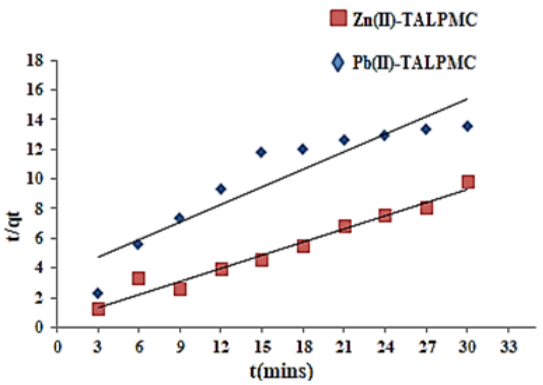

Fig. 27. Pseudo-Second Order Kinetics

Influence of TALPMC on Industrial Effluent

Figures 28 & 29 display the potency of TALPMC as (92%) for Zn(II) and (88%) for Pb(II) ions at 30 mg and 40 mg and 15 min contact time. Subsequent drop in the curve pattern at increased dosage is observed in both the systems, which may be due to the saturation of active sites on TALPMC. Three successive cycles were performed to evaluate the desorbing and regenerating ability of TALPMC towards the collected wastewater from oil industry as displayed in Table 6. Thus, the adsorption values have minimal difference in the amounts adsorbed, disclosing the excellent reusability of material.

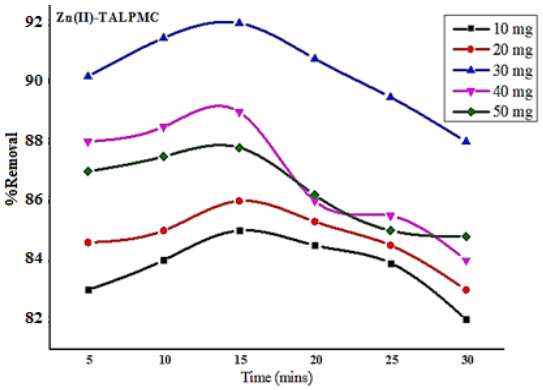

Fig. 28. Influence of TALPMC on Zn(II)

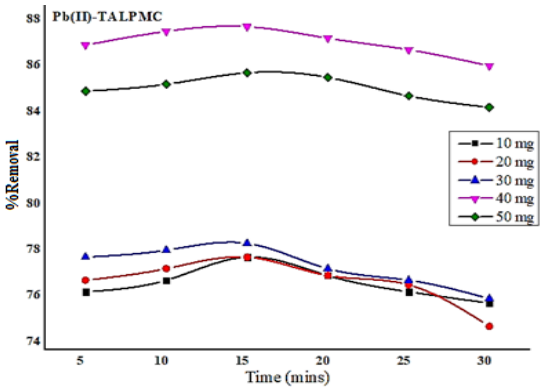

Fig. 29. Influence of TALPMC on Pb(II)

Table 6: Desorption/Regeneration Assay-Effluent

Systems	Cycle 1(mg/g) Adsorption	Desorption	Cycle 2 (mg/g) Adsorption	Desorption	Cycle 3 (mg/g) Adsorption	Desorption
Zn(II)-TALPMC	52.36	30.12	48.17	28.14	45.69	26.33
Pb(II)-TALPMC	46.32	33.56	42.54	35.32	40.96	38.55

Comparative analysis

Attraction of Zn(II) & Pb(II) onto the pores of magnetite sorbent surface opposite to TALP is due to the super paramagnetic property exhibited by the unpaired electrons present in Fe atom[16]. Moreover, TALPMC flashed up selective sorption of Zn^{2+} than Pb^{2+} ions. This can be accounted by the smaller ionic radius of Zn^{2+} (0.74Å than Pb^{2+}(1.33 A), resulting in its effortless confiscation of Zn(II). This is further corroborated by isothermal and kinetic constant values.

Mechanism

In TALP, the existence of functional groups viz., OH-, HPO_4^{2-} (Lewis bases) will bind with Zn(II) and Pb(II) (Lewis acids), enabling the sorption reaction[17]. In addition to the presence of OH-, HPO_4^{2}, the strong electrostatic attraction between the cations (Zn^{2+} & Pb^{2+}) and negatively charged part of the magnetite[18] (O_4^{2-}) in TALPMC, promotes the divalent ions to get adsorbed effectively on the sorbent's surface. Also, the formation of complexes due to the prevalence of high ratio of exchangeable Ca^{2+} ions enhances mechanism[17].

CONCLUSION

Magnetite composite was prepared by co-precipitation technique, employing Anas platyrhyncos Legs. Magnetic characteristics of Fe_3O_4 encapsulated Treated Anas platyrhyncos legs (TALPMC) solid matrix was validated via various analytical techniques like BET/BJH, FT-IR, SEM/EDAX, TG-DTA and XRD, to evaluate its nature during the sorption reaction. Batch experimentation exposed TALPMC as a promising sorbent for Zn(II) and Pb(II) removal from aqueous environs with maximal chelation of 97% and 95% than TALP (89% Zn^{2+} & 85% Pb^{2+}) under pre-fixed parametric conditions. Among the three isothermal models, Langmuir plot fitted well, suggesting monolayer sorption and Pseudo second order kinetics exhibited better linearity. Pilot study was conducted for the oil effluent sample, which produced satisfactory results by seizing 92% Zn(II) and 88% Pb(II) ions using TALPMC. The recorded outcomes and observations reveal that, magnetite biosorbent plays a prominent role in the sequestration of divalent metal ions both from aqueous and industrial effluent.

SOURCE

- Figs. 1-4 documented in this article were captured from experimental set up carried out in the chemistry lab in PSGR Krishnammal College for Women
- Figs. 5a-5c microscopic images, Binocular Ultrasound microscope (OLYMPUS make, Model-CX21I), figs 9a & 9b IR spectra (Shimadzu) and fig 14 Thermogram, TG/DTA (NETZSCH JUPITOR STA 449F3) recorded in PSGR Krishnammal College for Women
- Fig. 6-8 BET/BJH plots recorded in Material

Analysis & Research Centre, Bangalore

- Fig. 15, XRD pattern (Bruker D8 Advance make) recorded in VIT, Vellore
- Graphs (Fig 16a-29), computation, Origin 8.5 software
- Figs. 16a-22, 25 & 26, results of Batch Optimization studies
- Figs. 23-25 graphs of data derived from isothermal constants
- Figs. 28 & 29, graphic representation of kinetic constants calculated from corresponding equations.

ACKNOWLEDGEMENT

Authors acknowledge the DST FIST, New Delhi, India for the infrastructure provided.

Conflict of Interest

The authors declare no conflict of interest

REFERENCE

1. Behzadian, K.; Kapelan, Z., *Resour. Conserv. Recyc.*, **2015**, *99*, 84–99.
2. Yuanan Hu.; Hefa Cheng., *Environ. Dev.*, **2013**, *8*, 57-73.
3. Deblina Dutta.; Shashi Arya.; Sunil Kumar., *Chemosphere.*, **2021**, *285*, 131245.
4. Jebin Ahmed.; Abhijeet Thakur.; Arun Goyal., *RSC.*, **2021.**
5. Jessica Briffa.; Emmanuel Sinagra.; Renald Blundell., *Heliyon.*, **2020.**
6. Kosar Hikmat Hama Aziz.; Fryad S. Mustafa.; Khalid M., Omer., *RSC Adv.*, **2023**, *6*
7. Gessesse Kebede.; Tekle Tafese.; Ebrahim M. Abda.; M. Kamaraj, and Fassil Assefa., *J. Chem.*, **2021.**
8. David Molden., *Int. J. Water Resour. Dev.*, **2020**, *36.*
9. Amer Charbaji., *JMMCE.*, **2021**, *09*(03), 257-270.
10. Sasireka Velusamy.; Anurag Roy.; Senthilarasu Sundaram., *Chem. Rec.*, **2021.**
11. Narendra Singh.; Jinhui Li., *Adv. Mat. Res.*, **2013**, *878.*
12. Aliyu Haruna Sani.; Amanabo Musa., *Biol. Pharm. Sci.*, **2021.**
13. Nleya Y.; Simate GS.; Ndlovu S., *J. Clean. Prod.*, **2016**, *113*, 17-27.
14. Shagun Kainth A.; Piyush Sharma., *Appl. Surf. Sci. Adv.*, **2024**, *19*, 100562.
15. Nahum Andres Medellin-Castillo.; Miguel Mauricio Aguilera-Flores & Bridinette Thiodjio Sendja., *Springer, Porous. Mater.*, **2021**, 272-314.
16. Attarad Ali.; Hira Zafar.; Muhammad Zia.; Ihsan Ul Haq.; Abdul Rehman Phull.; Joham Sarfraz Ali, and Altaf Hussain., *Nanotechnol, Sci . Appl.*, **2016.**
17. Sarah Diallo-Garcia.; Manel Ben Osman.; Jean-Marc Krafft.; Sandra Casale.; Cyril Thomas.; Jun Kubo, and Guylène Costentin., *J. Phy. Chem.*, **2014**, *118*, (24), 12744–12757.
18. Fawzia I. El-Dib.; Dalia E. Mohamed.; Omnia A.A. El-Shamy.; Marwa R. Mishrif., *Egypt.J. Pet.*, **2020**, 1-7